Reducing anionic surfactant adsorption using polyacrylate as sacrificial agent investigated by QCM-D

Liu, Zilong; Hedayati, Pegah; Ghatkesar, Murali K.; Sun, Weichao; Onay, Hayati; Groenendijk, Dirk; van Wunnik, Johannes; Sudhölter, Ernst J.R.

DOI
10.1016/j.jcis.2020.11.090

Publication date
2021

Document Version
Final published version

Published in
Journal of Colloid and Interface Science

Journal of Colloid and Interface Science 585 (2021) 1–11

Contents lists available at ScienceDirect

Journal of Colloid and Interface Science

journal homepage: www.elsevier.com/locate/jcis

Regular Article

Reducing anionic surfactant adsorption using polyacrylate as sacrificial agent investigated by QCM-D

Zilong Liu [a,b,*], Pegah Hedayati [b], Murali K. Ghatkesar [c], Weichao Sun [d], Hayati Onay [b], Dirk Groenendijk [e], Johannes van Wunnik [e], Ernst J.R. Sudhölter [b,*]

[a] Beijing Key Laboratory of Optical Detection Technology for Oil and Gas, College of Science, China University of Petroleum (Beijing), Beijing 102249, China
[b] Organic Materials & Interfaces, Department of Chemical Engineering, Faculty of Applied Sciences, Delft University of Technology, Van der Maasweg 9, 2629 HZ Delft, the Netherlands
[c] Micro and Nano Engineering Group, Faculty of Mechanical Maritime and Materials (3mE) Engineering, Delft University of Technology, Mekelweg 2, 2628 CD Delft, the Netherlands
[d] Nano-Science Center, Department of Chemistry, University of Copenhagen, Universitetsparken 5, 2100 Copenhagen, Denmark
[e] Shell Global Solutions International B.V., Shell Technology Centre Amsterdam (STCA), Grasweg 31, 1031 HW Amsterdam, the Netherlands

GRAPHICAL ABSTRACT

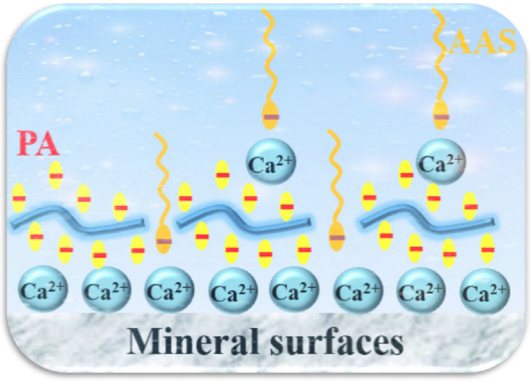

ARTICLE INFO

Article history:
Received 24 October 2020
Revised 15 November 2020
Accepted 23 November 2020
Available online 26 November 2020

Keywords:
Surfactant flooding
Polyelectrolyte
Divalent cation
Enhanced oil recovery
QCM-D

ABSTRACT

Surfactant losses by adsorption to rock surfaces make surfactant-based enhanced oil recovery economically less feasible. We investigated polyacrylate (PA) as a sacrificial agent in the reduction of anionic surfactant adsorption with focus on calcite surfaces by using quartz crystal microbalance with dissipation monitoring. It was found that the adsorption of the anionic surfactant alcohol alkoxy sulfate (AAS) followed a Langmuir adsorption isotherm, and the adsorbed amount reached saturation above its critical micellar concentration. Adsorption of PA was a much slower process compared to AAS adsorption. Increasing the calcium ion concentration also increased the amount of AAS adsorbed as well as the mass increase rate of PA adsorption. Experimental results combined with density functional theory calculations indicated that calcium cation bridging was important for anionic surfactant AAS and PA adsorption to calcite surfaces. To effectively reduce the amount of surfactant adsorption, it was needed to preflush with PA, rather than by a simultaneous injection. Preflushing with 30 ppm of PA gave a reduction of AAS adsorption of 30% under high salinity (HS, 31,800 ppm) conditions, compared to 8% reduction under low salinity (LS, 3180 ppm) conditions. In the absence of PA, the amount of adsorbed AAS was reduced by already 50% upon changing from HS to LS conditions. Lower calcium ion concentrations, as under LS conditions, contributed to this observation. On different mineral surfaces, PA reduced the AAS adsorption in

* Corresponding authors at: Beijing Key Laboratory of Optical Detection Technology for Oil and Gas, College of Science, China University of Petroleum (Beijing), Beijing 102249, China (Z. Liu).
E-mail addresses: zlliu89@gmail.com (Z. Liu), E.J.R.Sudholter@tudelft.nl (E.J.R. Sudhölter).

https://doi.org/10.1016/j.jcis.2020.11.090

the order of alumina > calcite > silica. These results offer important insights into mitigating surfactant adsorption using PA polyelectrolyte as sacrificial agent and contribute to improved flooding strategies with reduced surfactant loss.

1. Introduction

With the growing demand for oil production and achieving more efficient extraction of residual oil from petroleum reservoirs, tertiary oil recovery, also known as enhanced oil recovery (EOR), has been receiving substantial attention [1,2]. One of the more promising methods is chemical EOR (cEOR), which is the process of injecting chemicals (polymers, alkalis, and surfactants) into the reservoirs. Ample amounts of injected solutions contribute to the formation of micro emulsions through substantially lowering interfacial tension between oil and water, altering the mineral wettability, and producing foam for an improved sweep efficiency [1,3–6]. The major issue that reduces the recovery efficiency in cEOR is surfactant losses owing to adsorption to the rock surfaces [7,8]. Strong surfactant adsorption results in their chromatographic retardation when surfactants are carried through the pores of the reservoir rocks, rendering the cEOR process unproductive and commercially less viable [9]. To realize effective transport of surfactants through reservoir rocks, it is of great significance to investigate the factors affecting surfactant adsorption and with this knowledge to optimize the flooding conditions to arrive at a reduced surfactant loss.

In the surfactant-water-mineral systems, the amount of surfactant adsorption relies on the rock composition, surfactant properties, solution chemistry (*i.e.*, salinity, ionic composition, and pH), and the reservoir temperature [4,5,10–14]. Several experimental studies covering different aspects of surfactant adsorption processes have been investigated and mainly include adsorption kinetics [6], adsorption isotherms [10], adsorption mechanisms [12], and structures of surfactant layers [15–17]. A vast majority of research has been focused on minerals typical for sandstone (silica) reservoirs. However, approximately 60% of the world's oil reservoirs are found in carbonate fields (limestone, chalk, and dolomite) [18]. Bearing in mind the mineralogical differences, carbonate rocks could undergo dissolution, recrystallization, and mineralogical replacement, which make the investigation of adsorption on carbonate rocks to be more complex compared to sandstone surfaces. It has been shown that the adsorption of ionic surfactants on charged rock surfaces is strongly pH dependent [4,6]. Around neutral pH, silica has a negatively charged surface, while calcite, alumina, and dolomite surfaces are primarily positively charged [2,19]. Traditionally, added alkali like sodium carbonate has been used to increase the local pH, and therefore increasing the negative charge density of the surface, which leads to a reduction of anionic surfactant adsorption [20].

Another important factor influencing the surfactant adsorption to rock surfaces is the ionic compositions of the surfactant flooding solution [21–23]. Divalent cation, such as Ca^{2+}, is capable of acting as ionic bridges between anionic surfactants and negatively charged surfaces, and therefore favoring anionic surfactant adsorption [23–25]. On silica surfaces, it was shown the quantity of sodium dodecyl sulfate adsorption doubled when the contained (monovalent) sodium ions were substituted by (divalent) calcium ions [26]. A higher calcium ion concentration in the solution enhances the amount of adsorbed calcium ions in the Stern layer of the silica surface as deduced from the observed increase of zeta potential [11]. It is also usually observed that the adsorption of anionic surfactants increased with higher salinities and higher divalent cation concentrations in the solution [8,27]. The exchange of monovalent ions near the rock surface by divalent cations coming from the flooding solutions promotes the adsorption of anionic surfactants [23]. A cEOR process combining the injection of low salinity (LS) water and surfactant has been proven to be more effective compared to only LS or only surfactant flooding [28,29]. The dominant role of present divalent cations near silica and aluminosilica surfaces was also demonstrated under LS water flooding conditions by varying its concentration [24,30].

In order to extend the reduction of anionic surfactant adsorption to reservoir rocks, addition of anionic polyelectrolytes as the sacrificial agent can be very useful, because they compete with anionic surfactants for the rock surface binding sites. Since the final loss of such sacrificial agents is less expensive compared to surfactants, the use can be cost effective. Lignosulfonate polyelectrolytes have been applied successfully as an inexpensive preflush chemical to reduce the loss of anionic surfactants [31]. Also sodium polyacrylate of molecular weight (MW) > 4500 g/Mol is able to significantly reduce anionic surfactant adsorption on both Berea sandstone and Carlpool dolomite rock [32]. A different relationship between polymer MW and surfactant adsorption was found for poly(ethylene oxide), increasing the MW of poly(ethylene oxide) caused a reduction of cationic surfactant adsorption on silica [33]. The addition of polystyrene sulfonate has been shown to inhibit the adsorption of anionic surfactants at high saline conditions [25]. It was reported that the cationic polyelectrolyte polydiallyl dimethylammonium chloride was able to lower anionic surfactant adsorption [34]. To minimize surfactant adsorption, the use of polyelectrolytes has been evaluated onto high surface area minerals (mainly calcite, dolomite, quartz, and illite) [35]. Also the specific counterions (bromide, chloride, *etc.*) have an important effect on the co-adsorption of polyelectrolytes and surfactants onto silica surfaces [36]. The sequence of flushing surfactants and polyelectrolytes was found to be important on the effectiveness of the reduction of surfactant loss. A preflush with only polyelectrolytes, followed by surfactant injection, has been found to be more effective compared to an injection of a mixture of surfactants and polyelectrolytes [34,37]. Although various aforementioned polyelectrolytes have been proposed to reduce the surfactant adsorption, the dynamic adsorption process is not yet completely understood.

In this study, we have investigated in detail the adsorption behavior of a commonly used anionic surfactant alcohol alkoxy sulfate (AAS) and the anionic polyelectrolyte polyacrylate (PA) both applied separated and in combination. PA is of interest because it is a polyanion that is able to bind to mineral surfaces in competition with surfactants. Often we observed a high surface coverage and a slow desorption. Using quartz crystal microbalance with dissipation monitoring (QCM-D), the dynamic adsorption process of both AAS and PA can be easily monitored in real-time by recording the shifts in the resonant frequency of the quartz crystal for the first time. The frequency shift can be related to a change in adsorbed/desorbed mass [19,38,39]. The experiments described in this study were mainly performed on the calcite coated crystal as a model for carbonate rocks, and parts of the results were compared to results obtained from using silica and alumina surfaces. We have chosen harsh solution conditions, like high salinity (HS) and high hardness (high calcium ion content)

to mimic real surfactant flooding conditions. For comparisons some experiments were performed under low salinity (LS) conditions. Finally, we have identified the efficiency of using PA to reduce anionic AAS surfactant adsorption.

2. Experimental section

2.1. Chemicals and solutions

The anionic AAS surfactant having a MW = 700 g/Mol was supplied by Shell Global Solutions, which contains primarily C_{12} or C_{13} alkyl tails connected *via* seven propoxy units to a head group of ether-sulphate. Such an AAS surfactant is widely applied in cEOR with excellent divalent cation tolerance and is relatively inexpensive in comparison with other types of EOR surfactants [40]. Poly (acrylic acid, sodium salt) (PA, MW = 8,000 g/Mol) is a polyanion obtained from Sigma Aldrich. The molecular structures of AAS and PA are shown in Fig. 1*a*, and all compounds were utilized as received. Salt solutions were made by blending ultrapure deionized water (Milli-Q, resistivity of >18.2 MΩ·cm) with the appropriate amount of NaCl (500 mM) and $CaCl_2$ (0–100 mM), which were obtained from Sigma Aldrich and had purity grades of >99.0%. To prevent the dissolution of the used calcite sensors, the Milli-Q water was pre-equilibrated with an aqueous 0.1 mM $CaCl_2$ solution, a slightly higher concentration than the equilibrium concentration of Ca^{2+} in a calcite solution [41]. The prepared surfactant solution was made by dissolving the appropriate amount of AAS with the aqueous salt solution and the solution pH was regulated to the desired value with a Metrohm 827 pH meter.

2.2. Coated QCM-D crystals

The quartz crystals coated with calcium carbonate ($CaCO_3$, QS-QSX 999), silicon dioxide (SiO_2, QS-QSX 303), and aluminum oxide (Al_2O_3, QS-QSX 309) were purchased from Biolin Scientific. It has an AT-cut quartz crystal (0.3 μm in thickness and area of 0.2 cm^2, see the inset in Fig. 1*b*) with a fundamental resonance frequency (f_0) of 5 MHz. Most experiments were performed on calcite coated sensors, and a few on silicon dioxide and aluminium oxide for comparisons. Before using these sensors, they were subsequently rinsed with ethanol and isopropanol, and mildly dried under the flow of nitrogen gas. Next, the sensors were mounted to the flow module and adapted to the appropriate position. The reuse of the sensors is determined by the obtained repeatability of the output signal during experiments. To alleviate the drift effects of signals, each sensor was utilized less than five times.

2.3. Surface characterizations and viscosity measurements

Atomic Force Microscopy (AFM) topography image of calcite surface was collected in tapping mode with a silicon tip (NSG03, NT-MDT) that had a nominal spring constant of 0.4–2.7 N/m and tip radius around 7 nm. The scan rate was 1 Hz. As shown in Fig. 1*b*, the calcite surface is very smooth, with a low surface roughness of 1.52 nm of root mean square height. The silica and alumina coated sensors showed similar roughness as calcite, which was consistent with previously obtained results [39]. A JSM-IT200 Intouchscope™ scanning electron microscope (SEM) from JEOL was used to study the larger morphology of sensors. The SEM images was obtained under high voltage and high vacuum conditions at magnifications up to 1000 times (*Figure S1*). The viscosity properties of studied solutions were characterized by oscillation shear rheometry (Physica MCR 501 rheometer, Anton Paar) with a cone-plate geometry. The reported viscosity data are the averaged values of three measurements. The obtained results are shown in *Figure S2*. The determined viscosity differences at room temperature between HS (50 mM $CaCl_2$ with 500 mM NaCl, 31,800 ppm), HS with 0.15 wt% AAS (2.1 mM, which was well above its CMC), and HS with 0.15 wt% AAS and 30 ppm PA are less than 0.04 mPa·s. The viscosity curves of HS + AAS and HS + AAS + PA are almost overlapped. Therefore, any effect of bulk viscosity change on frequency shift can be excluded.

2.4. QCM-D principle

The adsorption behavior of surfactants was investigated using a QCM-D (E1, Q-sense), which measured the change in resonance frequencies and dissipations of the coated quartz crystals. When an alternating current is employed to the electrodes, shear stress is generated because of the piezoelectric property of quartz, leading to the oscillation of the crystal at its fundamental resonance frequency (f). The shift in f was recorded when the oscillating crystal contacted with an aqueous solution, which was the result of the next three contributions: mass loading (*Eq.* (1)), [42] liquid loading

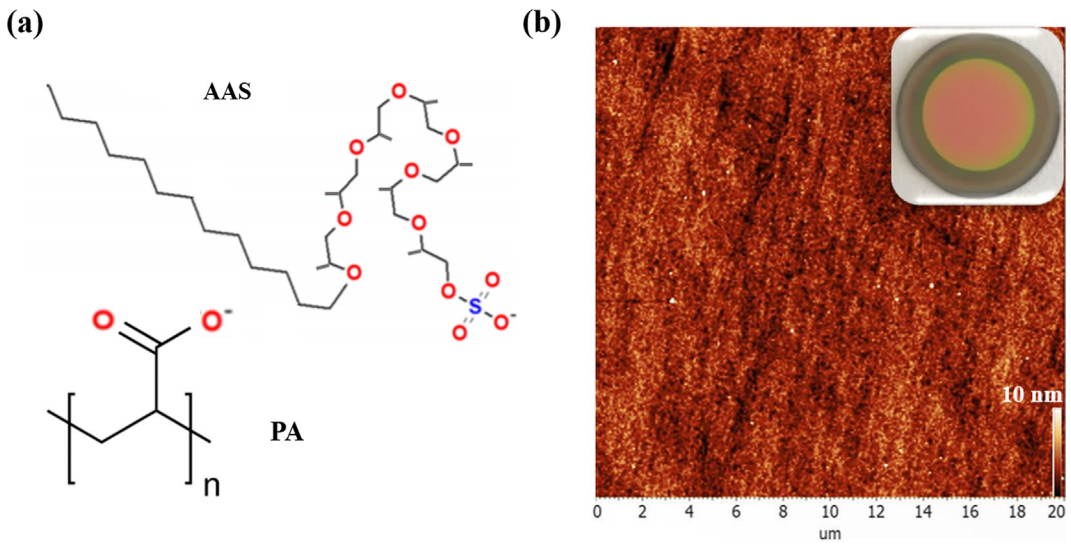

Fig. 1. (a) The molecular structure of used AAS surfactants and PA polyelectrolytes (n = 85). (b) AFM topography image (20 × 20 μm^2) of calcite modified sensor surface. The inset is the calcite modified sensor (14 mm in diameter) used for QCM-D surfactant adsorption measurements.

(*Eq.* (2)), [43] and liquid trapping (*Eq.* (3)), [44] described by the equations below.

Mass loading (Sauerbrey equation):

$$\Delta f_{ads} = -\frac{2nf_0^2\Delta m}{\rho_q v_q} = -\frac{n\Delta m}{C} \quad (1)$$

Liquid loading:

$$\Delta f_{liquid\ \ loading} = -\sqrt{\frac{n}{\pi}}\frac{2f_0^{1.5}}{\rho_q v_q}(\sqrt{\rho_1\mu_1} - \sqrt{\rho_2\mu_2}) \quad (2)$$

Liquid trapping:

$$\Delta f_{liquid\ \ trapping} = -\frac{2f_0^2}{\rho_q v_q}h_l(\rho_l - \rho_s) \quad (3)$$

where Δm is the adsorbed mass, f_0 is the fundamental resonant frequency, n = 1, 3, 5, is the overtone number, C is the mass-sensitivity constant of 17.7 ng/cm^2/Hz, $\rho_q$is the specific density (2650 kg/m^3), v_q is the shear wave velocity (3,340 m/s), h_l is the thickness of the trapped liquid. Subscripts 1 and 2 refer to different solution densities and viscosities, whereas the subscripts s and l refer to the solvent and liquid mixtures, respectively. The adsorbed mass of a thin, rigid, uniformly distributed layer can be calculated with *Eq. (1)*. When Newtonian fluids flow over the crystal, the frequency shifts because of the changes in viscosity and density of injected solution were estimated with *Eq. (2)*. The surface roughness of the quartz crystal can also influence the frequency shift due to the liquid trapping by interfacial cavities and pores, [45] and this contribution was calculated using *Eq. (3)*. However, this effect of liquid trapping was neglected, because all our used sensors were atomically flat.

2.5. QCM-D experimental procedures

Prior to each experiment, the contacting parts of the flow module were also rinsed by following the same procedures as for cleaning the coated sensor. All experiments were conducted at 23 ± 0.1 °C and at a constant flow rate of 200 μL/min. First, Milli-Q water equilibrated with aqueous 0.1 mM $CaCl_2$ solution was injected into the flow modules by using a peristaltic pump (ISMATEC, ISM935C). Simultaneously, the resonant frequency and dissipation shifts of different overtones of the crystal were monitored. It was observed that the fifth resonant frequency showed a better signal-to-noise ratio and was therefore selected in this work. The baseline was regarded to be stable if during a period of 10 min, the frequency change was less than ±1 Hz. If the reference signal (starting signal) was stable and reproducible, a salt solution was injected and then followed by continuous the surfactant solution injection. Next, the solution was exchanged to Milli-Q or salt solutions to see if the signal returns to the starting position. Each adsorption measurement was repeated 2 to 4 times to ensure the accuracy and reliability of the obtained results. Finally, Milli-Q water was flushed for 45 min to rinse the entire system. The density and viscosity of the salt solutions were found to be similar to the salt solutions in the presence of 0.15 wt% (2.1 mM) surfactant, therefore the liquid loading effect was neglected (see Sections 2.3 and 2.4). The quantity of adsorbed surfactants was calculated by the frequency difference between salt and surfactant solutions, *i.e.*, $\Delta f_{ads}(surfactant) = \Delta f_{surfactant+salt} - \Delta f_{salt}$. The averaged values were taken and used for the calculations.

2.6. Density functional theory (DFT) calculations

Using DFT calculations the binding energy values among various functional groups can be estimated. These calculations were performed to compare the cation bridging capabilities of AAS and PA carrying a cation (Na^+ and Ca^{2+}) to the calcite surface. DFT calculations were performed with the TURBOMOLE program (v6.5), [46] using the Becke-Perdew functional, [47,48] the triple-ζ valence plus polarization basis set, [49] and the COSMO implicit solvent model [50]. All the binding energies for the complexes were calculated by subtracting basis superposition errors using the counterpoise correction provided in TURBOMOLE program. To model PA in its anionic state, deprotonated octanoate was used, where the terminal six carbon atoms were fixed during the optimization [24,25,51]. The possible configurations of octanoate molecules can be present in a monomer and/or dimer, such as octanoate-Ca^{2+}-octanoate. Such simplified dimer configurations may interact to calcite surfaces because of an unevenly charge distribution [51]. Using the same method, the AAS surfactant was modeled by replacing the carboxylate group in octanoate with a sulfate or a propoxy group, mimicking the functional groups of AAS. Here, we were interested in the binding strengths between carboxylate, sulfate and propoxy groups, and calcite surfaces via a cation bridging. Thus, the interactions between these groups to mineral surfaces and the interactions in solutions containing cations (Na^+ and Ca^{2+}) were calculated. The differences between interaction energy to mineral surface and in solution, *i.e.* the binding energies, were calculated for both monomers and dimers, as shown in Fig. 2. Ion bridging would take place if the binding energy is negative, which contributes to a favoured adsorption. A much smaller relative value of the binding energy is expected for the monovalent ions (Na^+) in comparison to the divalent ions (Ca^{2+}), since the monovalent ions are not capable to form cation bridges to the surface.

3. Results and discussions

3.1. Adsorption behavior of AAS and PA

We first investigated the separate adsorption of AAS and PA on calcite sensors by using QCM-D at room temperature (23 ± 0.1 °C) in aqueous 50 mM $CaCl_2$ at pH = 9.5. The observed frequency shifts were plotted as a function of time for the different applied AAS and PA concentrations (Fig. 3*a and c*). In addition, the maximum amounts of AAS adsorbed (in frequency shift values) were plotted as a function of their applied concentrations (Fig. 3*b*) and also the adsorption rates of PA at different applied concentrations (Fig. 3*d*).

As shown in Fig. 3*a, a* larger frequency shift was observed when changing from only salt solution to an AAS containing solution,

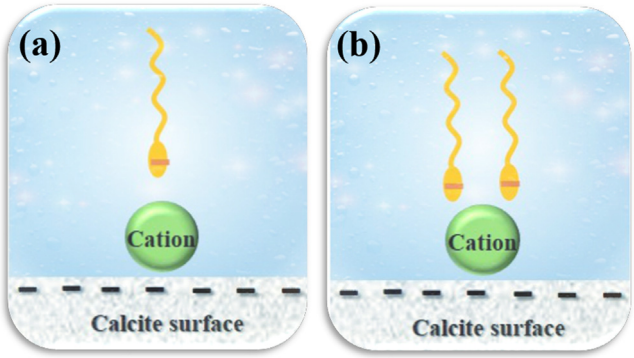

Fig. 2. Schematic representation of the monomer (a) and dimer (b) of surfactant AAS or PA polyelectrolyte model molecules binding a cation ion (Na^+ or Ca^{2+}) to the calcite surface. The difference in interaction energies between the monomer/dimer in the water phase and to the calcite surface was used to estimate the likelihood of cation bridging.

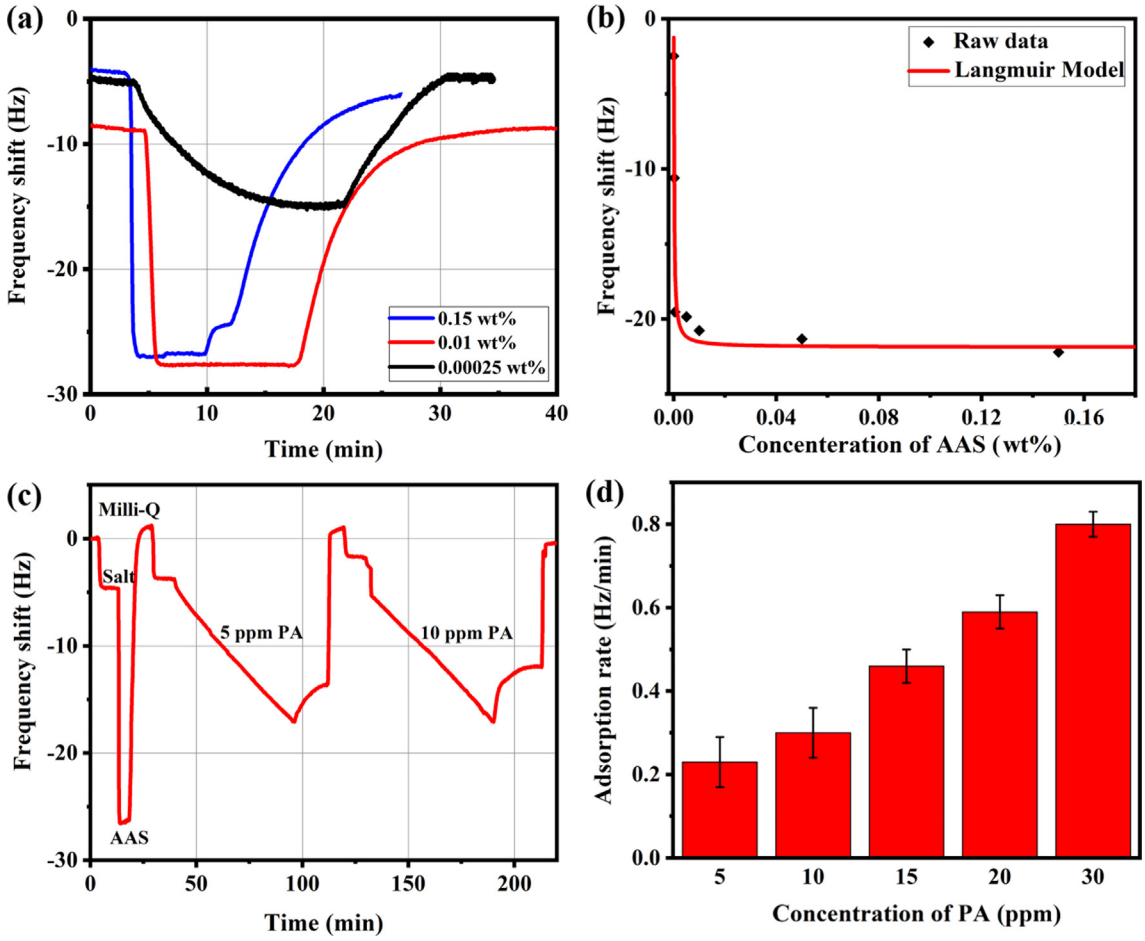

Fig. 3. Real-time frequency shifts for the adsorption of (a) AAS and (c) PA at different applied concentrations. In the desorption process, firstly flushing with the salt solution for AAS and PA, and next with Milli-Q water only for PA gave a complete desorption. The maximal frequency shift observed as function of the applied concentration of (b) AAS and (d) the adsorption rate as function of the concentration of PA. The data for AAS adsorption were fitted according to the Langmuir adsorption model (b, solid line). The unit conversion: 1 wt% = 10,000 ppm.

which was interpreted as an increased AAS adsorption on the calcite modified sensor surface. With an increase of AAS concentration, a larger frequency drop was observed (Fig. 3*a and S3*). The maximum frequency shift (the maximal amount of adsorbed AAS) was found at an applied AAS concentration around 0.02 wt % (=0.3 mM, Fig. 3*b*), which is about four times the critical micelle concentration (CMC ~0.005 wt%, 0.07 mM). The observed increase of AAS adsorption above the CMC of AAS indicates that the affinity of AAS monomer to the surface is slightly higher compared with their affinity towards micelles. It might also be that the presence of impurities in the technical grade AAS contributes to this observation. Adsorption of AAS stopped as the surface was occupied. The Langmuir model was applied to the adsorption isotherm, and all the data showed a good correlation with the Langmuir equation that had an observed regression coefficient larger than 0.96, as is shown in Fig. 3*b*. From the applicability of the Langmuir model, it can be concluded that the AAS adsorption affinity on calcite surfaces is independent of the coverage of already adsorbed AAS. Likely, the interaction between the AAS head group and the surface via calcium ion bridging is thus much more dominant compared to the expected favorable mutual alkyl-alkyl interactions.

Based on the obtained maximal frequency shift of ~23 Hz (Fig. 3*b*), the calculated mass increase was 4.1 mg/m^2, by using the mass-sensitivity constant of 17.7 ng/cm^2/Hz for the used quartz crystal (see Section 2.4). Using the molecular weight of AAS of 700 g/Mol, this mass equals to 5.9 $\times$ 10^{-6} Mol/m^2 = 3.5 molecules/nm^2. Since the AAS adsorbs to the surface in contact with an aqueous environment, it is likely that a bilayer of AAS is formed. For a tightly packed monolayer a single molecule occupies an area of 0.40 nm^2, [52–54] it is therefore clear that in our situation a loosely packed bilayer has been formed. Looking into the AAS desorption process (as deduced from the slope of the desorption curve) after AAS adsorption from a 0.15 wt% solution (blue curve, Fig. 3*a*), we always observed a two-step process with first a small and fast desorption (2.3 Hz/min), followed by somewhat slow and more gradual increase towards the final baseline. The first process (a small step in the blue curve of Fig. 3*a*) was likely ascribed to the release of weakly adsorbed AAS outer surfactant molecules. Desorption of AAS from a lower concentration solution showed only a single desorption process (0.01 wt% red and 0.00025 wt% black curve, Fig. 3*a*). Looking also here to the slopes of the desorption curves, it is seen that for the second desorption step for 0.15 wt% (blue) and for 0.01 wt% (red) the slopes are more or less similar, while for 0.00025 wt% (black) the slope (1.1 Hz/min) is higher, but not as high as observed for the first desorption step of 0.15 wt% (2.3 Hz/min). This observation might point to AAS desorption from a loosely packed monolayer directly bound to the sensor surface.

Another remarkable observation is that the adsorption rates (~15 Hz/min) observed for 0.15 wt% and 0.01 wt% of AAS are fast compared to the much slower adsorption rate (0.7 Hz/min) observed for 0.00025 wt% AAS. We interpret this difference by

the difference in free monomer AAS concentration, which is in the first two cases similar to the CMC and thus more or less constant, while for the last situation the free monomer is below the CMC. Therefore, in that case the AAS monomer concentration gradient to the surface is lower, and a lower adsorption rate is expected. The quality of the used calcite sensors was checked several times by a reference adsorption experiment (Section 2.5). This is because a tiny amount of calcite might easily go into solution and therefore destroy the sensor surface. The reference experiment was performed using 50 mM $CaCl_2$ solution containing 0.15 wt% AAS, at pH = 9.5 and room temperature. Only sensors showing reproducible results were reused.

Next, we describe the adsorption experiments of PA. Also for these experiments, the quality of the calcite sensor was first checked as described above (Fig. 3*c*). The presence of a small amount of PA (5–30 ppm) in the 50 mM $CaCl_2$ solution at pH = 9.5 showed, in contrast to the observed fast adsorption for AAS, a slow and continuous mass increase during our observation time of about 90 min. The adsorption rate of 5 ppm (0.63μ M) PA was around 0.2 Hz/min that was much slower in comparison with the observed adsorption rate for AAS (15 Hz/min). The PA adsorption rate is therefore about 75 times slower in comparison with the adsorption rate of AAS. After a period of 115 min the same amount of adsorbed mass of PA is observed (23 Hz frequency shift) as compared to amount of adsorbed mass of AAS after about 1 min (using AAS concentrations >CMC). In contrast to AAS, this slow PA adsorption did not stop and continued for at least 300 min (*Figure S4*). This continuous PA adsorption indicates the formation of adsorbed multilayers, likely formed via calcium ions bridging between the carboxylate groups of successive PA layers. The approximate mass adsorbed after 300 min for PA is 25.5 mg/m^2 that is six times more than a bilayer from AAS adsorption. A small sharp frequency shift (1–3 Hz) was also observed when salt solution was changed to PA solution, and it might be attributed to small solution viscosity differences. The solutions containing such low concentrations of PA (5–30 ppm) and such high $CaCl_2$ concentrations (50 mM) did not show any visible precipitations during our experiments. It was reported that for low PA concentrations, the introduction of Ca^{2+} led to the formation of stable coiled configurations of PA [55,56]. The observed slow adsorption rate of PA compared to the fast adsorption observed for AAS is likely attributed to (1) the higher MW of PA (8000 g/Mol) compared to AAS (700 g/Mol), making diffusion through the stagnant layer a slower process; (2) the differences in applied concentrations. AAS is applied at a concentration below and above the CMC of 70 μM, and the PA concentrations are in the range of 5–30 ppm (0.63–3.75 μM). These much lower concentrations lead to a lower concentration gradient over the stagnant layer, and therefore to a lower driving force; (3) the possible complexation of PA with Ca^{2+} in the bulk phase would reduce its adsorption on the solid-liquid interface; (4) the adsorption rate of PA might in addition be reduced by a coil-extended conformational change upon binding [57–59].

Desorption of adsorbed PA to calcite surfaces was monitored by leaving out only the amount of PA in the added solution after an executed adsorption experiment. Only a small fraction (~20%) is desorbed in this way after 30 min. Upon flushing next with only Milli-Q water, desorption of the remaining PA is fast and also complete. Both the absence of calcium ions and the increased pH of Milli-Q (more negative surface charge of calcite) contribute to this observation. The whole procedure of adsorption and desorption was repeated and showed the same behavior. The complete reversibility of the adsorption process shows the dynamic behavior of the adsorbed PA multilayer. Applying a higher PA concentration, in the range from 5 to 30 ppm, showed an increase in adsorption rate, as expected (Fig. 3*d*). With the same time interval, the higher adsorption rate also contributes to a larger amount of adsorbed PA.

3.2. Effect of varying $CaCl_2$ concentrations on AAS and PA adsorption at high salinity conditions

Separate adsorption of AAS and PA to calcite sensor surfaces was investigated at room temperature, pH = 9.5 and 500 mM NaCl, to mimic HS conditions, with varying amounts of $CaCl_2$ (0–100 mM). The AAS concentration chosen was fixed to 0.15 wt% (2.1 mM). The PA concentration chosen was 20 ppm, which was similar to the concentration used for surfactant inhibition (*vide infra,* Section 3.3). All solutions investigated were clear solutions and no precipitation was observed during our experiments. The results obtained are shown in Fig. 4. Under the applied conditions and in the absence of added $CaCl_2$, AAS does adsorb, as deduced from the observed frequency shift of 22 Hz. Before, we have observed a similar frequency shift at 50 mM $CaCl_2$ and without any NaCl present. Adding now 50 mM $CaCl_2$ to the 500 mM NaCl solution, the frequency shift increased to ~32 Hz. From these comparisons, it is concluded that the presence of NaCl contributes to an increase of AAS binding. This likely happens via increased charge screening, resulting in a reduced electrostatic repulsion and hence increase binding.

To understand the interactions of AAS with the calcite surface under the different ionic conditions just described, DFT calculations were performed (Section 2.6). The binding energies between functional groups and calcite surfaces through a cation were calculated and the results are shown in Table 1. It was found that the relative binding energy in the presence of Ca^{2+} was always larger than in the presence of Na^+. It was suggested that on the calcite surface the binding sites for AAS surfactant was likely via calcium cation bridging, which was consistent with our experimental observations and previous findings [24,25,51]. The structures of calcium ions connected to a monomer and dimer of sulfate showed stronger binding to calcite surfaces compared to the structures derived from propoxy or carboxylate.

We had also extended our adsorption experiments to the silica surface in the presence of 500 mM NaCl and absence of $CaCl_2$ [60] The AAS surfactant adsorption was found to be negligible. Comparison with the observed high affinity of AAS to calcite surfaces at 500 mM NaCl, brings us to the conclusion that in that situation calcium ions near the calcite surface are not replaced by sodium ion, and accessible calcium ion sites on the calcite surface play a dominant role. The role of present sodium ion is therefore mainly to adjust the ionic strength of the solution and to enhance the surface charge screening.

Increasing the $CaCl_2$ concentrations above 50 mM shows an increased frequency shift indicating more AAS adsorption. At the highest investigated $CaCl_2$ concentration of 100 mM the frequency shift amounts to be 120 Hz. This indicates a four-fold increase of adsorbed mass. Since we have around 50 mM $CaCl_2$ one bilayer of AAS adsorbed, the current frequency shift suggests that now 4 bilayers may be adsorbed, assuming no corrugation of the surface. The interaction between the first bilayer and the second bilayer might be favored by calcium ion bridging between the opposing sulfate head groups. This interpretation is similar to the interpretation given for multilayer formation of PA. That multilayer formation of PA is more pronounced compared to AAS, is likely due to the cooperativity in PA multilayer formation where many negatively charged carboxylate anions are connected via the polymer backbone, which is absent in the singly negatively charged AAS surfactant molecules. A more detailed real-time adsorption/desorption process of AAS with varying $CaCl_2$ concentrations can be seen in *Figure S5*. A two-step desorption was also observed: an initial desorption of weakly adsorbed AAS surfactants, followed by the release of strongly bound AAS. In terms of previous study on clay surfaces, [53] calcium ions were always needed for the adsorption of AAS. However, for the calcite surfaces, added calcium ions

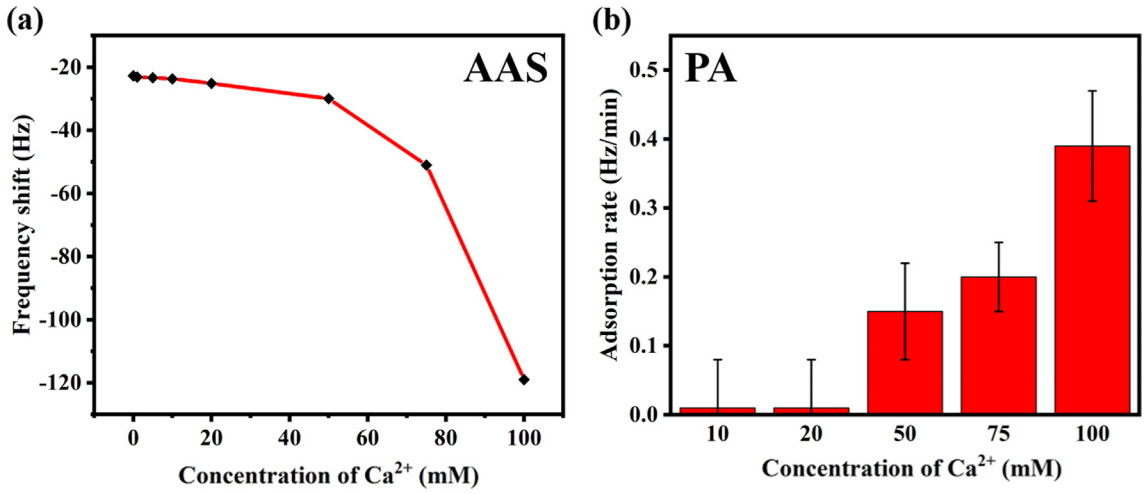

Fig. 4. Observed maximal frequency shifts for the adsorption of 0.15 wt% AAS (a) and observed adsorption rates for 20 ppm PA (b) both as a function of a varying $CaCl_2$ concentration (0–100 mM) in the presence of 500 mM NaCl. The unit conversion: 1 wt% = 10,000 ppm.

Table 1
The difference in binding energies (eV) between a monomer/dimer of model molecules carrying a cation (Na^+ or Ca^{2+}) from the water phase to the calcite surface.[a]

Model molecule	Na^+	Ca^{2+}
Sulfate_monomer	−0.76	−1.80
Sulfate_dimer	−0.83	−2.12
Propoxy_monomer	−0.31	−1.74
Propoxy_dimer	−0.41	−1.78
Carboxyl_monomer	−0.78	−1.58
Carboxyl_dimer	−0.65	−1.78

[a] The model molecules are chosen according to the presence of functional groups in AAS surfactant and PA polyelectrolyte.

were not necessary, because the calcite surface itself does supply these ions.

Now we come to the PA adsorption (20 ppm applied concentration) to calcite at pH = 9.5 under 500 mM NaCl, mimicking HS conditions, and varying $CaCl_2$ concentrations. As before the PA adsorption was a slow process in comparison with the AAS adsorption, and therefore also here the adsorption rates are presented. These adsorption rates were deduced from the slopes of the observed frequency shifts as a function of time. For all these experiments we have applied a time window of 90 min. The data are shown in Fig. 4*b*. For conditions of 10 and 20 mM Ca^{2+}, the PA adsorption was almost negligible and quite slow. Increasing the $CaCl_2$ concentration increases the rate of PA adsorption. For instance, in the presence of 50 mM $CaCl_2$ the PA adsorption rate is found to be 0.2 Hz/min and the rate increases to 0.4 Hz/min at 100 mM $CaCl_2$. More calcium ions in solution result in more calcium ions at the interface, and therefore more binding sites. Also for PA adsorption the process does not stop at a single polyelectrolyte adsorption, but continuous adsorption occurs (*vide supra*). If we compare the adsorption rate of PA in the presence of 50 mM $CaCl_2$ and 500 mM NaCl (0.2 Hz/min) with the adsorption rate in the absence of NaCl (0.6 Hz/min) we see that high concentrations of NaCl slow down the adsorption rate. If only charge screening plays a role, the reduced electrostatic repulsion would lead to an expected increased adsorption rate. Since we observe a decreased adsorption rate another effect is dominant. This is most likely the replacement of calcium ion binding sites near the interface by sodium ions, lacking any bridging properties (Table 1). Thus the ratio of $CaCl_2$ to NaCl concentration in the solution determines the number of calcium sites at the calcite surface, [58] which can act as a site for PA binding. The reduced adsorption rate of PA can also be originated from a salting-in effect of NaCl, favoring the PA solubility.

3.3. Effect of PA on AAS adsorption to calcite surfaces

We come now to the point of the effect of PA on the adsorption of AAS. This is of importance since surfactant loss in enhanced oil recovery processes is an essential issue. If it is possible to reduce the amount of adsorbed (=lost) AAS by the addition of minor amounts of PA, this could be of benefit to the process. Earlier, we have seen the different adsorption behavior of AAS and PA. AAS adsorbs to calcite surfaces in a fast way and stops adsorbing at a bilayer coverage. In contrast, PA adsorption is a very slow process and the adsorption continues to multilayer adsorption. Both adsorptions are completely reversible upon changing the flushing solution to Milli-Q water. To be able to observe any effect of PA on AAS adsorption, it is important that the calcite surface is first contacted with PA, and subsequently with AAS. That is because PA adsorption is slow and has less cation bridging compared to AAS adsorption (Table 1). Otherwise, AAS would adsorb immediately, and it would take a long time for PA to compete with AAS adsorbed. This is indeed what is observed for co-injection of mixed PA and AAS, and preflush with PA methods (*Figure S6*). If we flush directly with a mixture of PA and AAS, PA had a negligible effect for reducing AAS adsorption. (*Figure S7*) That PA adsorbs more strongly compared to AAS is expected based on the cooperativity of a polyelectrolyte binding (multiple anions in the same polymer chain) to a surface compared to a surfactant (single anion per molecule; only some cooperativities due to some alkyl chain-alkyl chain interaction in the adsorbed state). This is also the reason why such a low PA concentration is already effective compared to the CMC of the used surfactant. We have therefore investigated the changes in the frequency shift of calcite sensors at room temperature, pH = 9.5, 500 mM NaCl (to mimic HS conditions), 50 mM $CaCl_2$, 0.15 wt% AAS, after first flushing with varying PA concentrations in the range of 0 to 40 ppm (=5 μM). The results are shown in Fig. 5.

In a typical experiment, the calcite sensor quality was first checked as described in Section 3.1. We then repeated the experiment of AAS adsorption in the absence of any PA. The adsorbed amount reflected in the observed frequency shift of 32 Hz is as observed before (Section 3.2). The AAS is desorbed by injecting with Milli-Q water. The desorption occurs in a two-step way as dis-

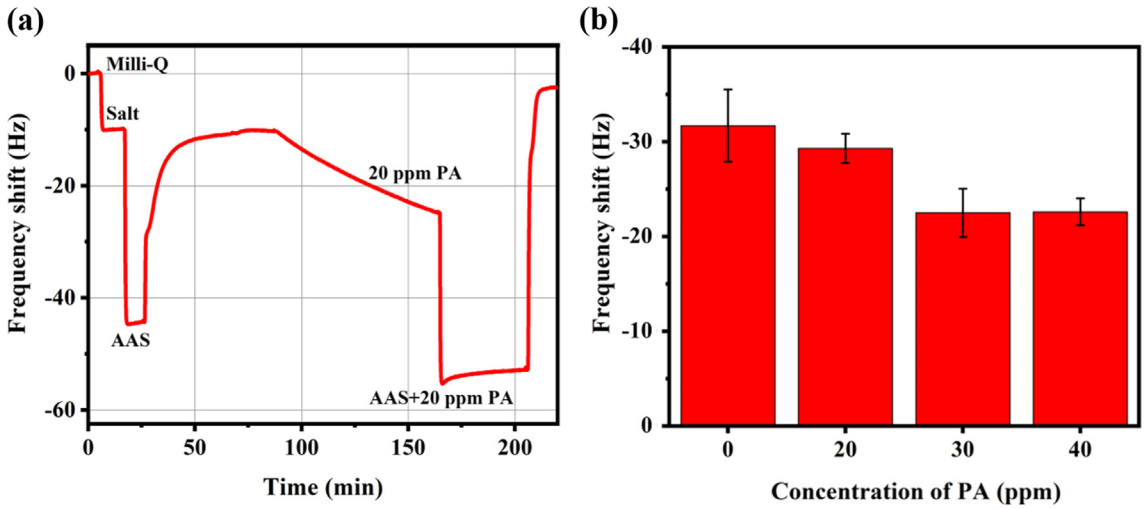

Fig. 5. (a) Real-time frequency shifts for the adsorption of AAS in the absence and presence of 20 ppm PA. (b) Observed frequency shifts for the AAS adsorption with a varied PA concentrations. All experiments were carried out with 0.15 wt% AAS and in the presence of 50 mM $CaCl_2$ and 500 mM NaCl, at pH 9.5 and room temperature. The unit conversion: 1 wt% = 10,000 ppm.

cussed before. Next, the PA solution of a 20 ppm concentration is applied during 90 min. Subsequently, the composition of the flushing solution is changed to PA solution but now containing 0.15 wt% AAS. A fast frequency shift is observed. The value of that shift is dependent on the amount of applied PA. We have varied the PA concentration during a fixed time interval of 90 min. Since the amount of PA adsorbed dictates the effect on AAS adsorption, you also may apply the same PA concentration during a longer tine interval, or to apply a higher concentration, during a shorter time interval. In our case we have observed that the amount of AAS adsorbed after preflushing with PA, decreases with the amount of PA applied (Fig. 5*b*). It is seen that the more PA is applied in the preflush, the less AAS is adsorbed. Clearly, the adsorbed PA to the calcite surface does inhibit the AAS adsorption. Applying for instance 30 ppm PA, does reduce the AAS adsorption from ~32 to 23 Hz and the maximal AAS adsorption reduction of about 30% is obtained. However, looking into more detail learns that the observed frequency shift was 15 Hz after flushing with 30 ppm PA for 90 min. This leads to a reduction of AAS adsorbed as expressed by a reduced frequency shift of 9 Hz. Therefore, the required amount of PA in terms of mass is roughly estimated to about 2 times higher than the amount of spared AAS. We also speculate that the reduction of AAS adsorption to the calcite surface originates from calcite surface sites already covered by PA (charge screening effect). The AAS still adsorbed to the PA covered calcite surface could be due to still available calcite surface sites and/or by AAS binding to top of the single PA layer via calcium ion binding.

3.4. Low salinity effect

The LS water flooding for further EOR has been proven to be useful, and triggers more oil released from reservoirs compared to conventional flooding with seawater or formation water [24,30,61]. Recently, a higher oil recovery was reported by applying a combination of surfactant and LS water injection method when compared with applying only LS or only surfactant flooding [28,29]. We described our results of the effect of PA (30 ppm) on the amount of AAS adsorbed under LS conditions and compared them with our results obtained for HS conditions (Section 3.3). To obtain LS (3,180 ppm) water, we diluted our HS solution, containing 50 mM $CaCl_2$ with 500 mM NaCl (31,800 ppm), 10 times with Milli-Q water, which was similar to those reported previously [24,53].

The different AAS adsorptions on calcite surfaces under LS and HS in the presence and absence of PA are shown in Fig. 6. At LS conditions, the observed adsorption rate for PA of 0.1 Hz/min was much slower compared to the previously described adsorption rate of ~0.2 Hz/min at HS conditions. It can be understood by the lower calcium cation concentration in the LS solution for the PA binding. A lower concentration gives less calcium binding sites at the surface. Flushing next with a mixture of PA and AAS under these LS conditions show that the amount of AAS adsorbed is less (15 Hz) compared to the amount adsorbed under HS conditions (32 Hz). Comparisons of these data with the adsorbed AAS in the absence of PA under LS and HS conditions, show that the reduction of AAS adsorption by the action of 30 ppm PA is 8% and 30% respectively. The reduction of both PA and AAS adsorption is most likely due to the lower calcium ion concentration under LS conditions. A comparison of AAS adsorption reduction by PA is overall more effective under HS conditions compared to LS conditions. In the absence of PA, the reduction of AAS adsorption was ~50% in LS compared to HS, which was found to be consistent with our previous results obtained for clay minerals [47]. We come now to the general conclusion that AAS adsorption to calcite surfaces can be reduced by switching from HS to LS conditions, or to preflush with PA at HS conditions.

3.5. Different mineral surfaces

The potential of PA to reduce AAS adsorption to calcite surfaces was also investigated on silica and alumina surfaces. We have chosen here also the PA concentration of 30 ppm being effective for calcite. After a PA preflush, the combination of PA and AAS were flushed to two different, silica and alumina, sensor surfaces. They showed a similar adsorption behavior as on the calcite surfaces. The rate of PA adsorption to silica and to alumina are about 1 and 1.2 Hz/min, respectively, which were higher than on calcite (0.2 Hz/min). PA reduced surfactant adsorption in an order of alumina > calcite > silica, as is shown in Fig. 7. This observation is consistent with the results from Hirasaki et al. [8,32], who observed that the reduction of surfactant blends adsorption due to the presence of PA was found to be larger for carbonate and clay compared to sandstones. They claimed that the decrease in adsorp-

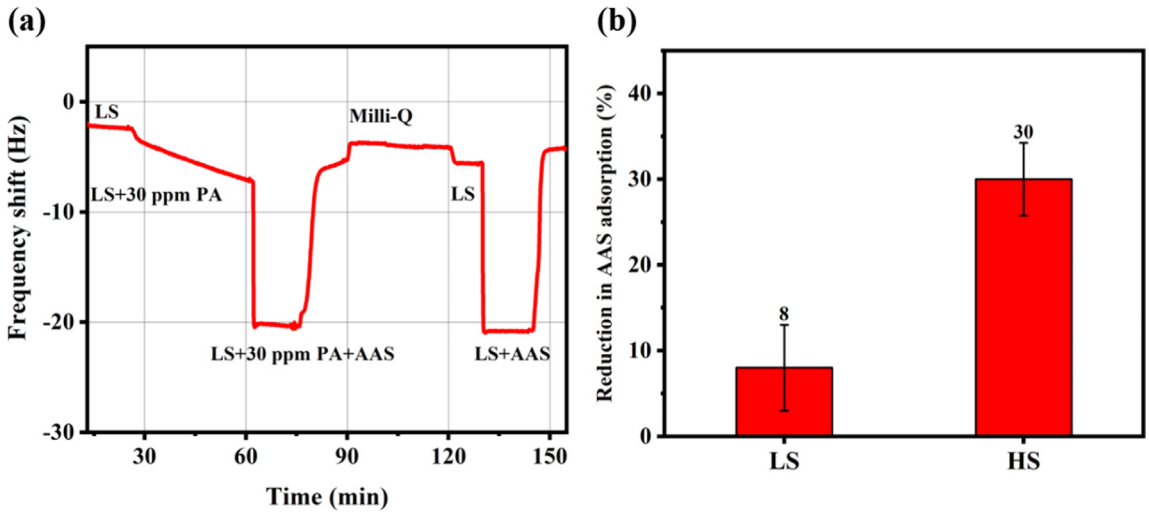

Fig. 6. (a) Real-time frequency shifts for the adsorption of 0.15 wt% AAS in the absence and presence of 30 ppm PA at LS conditions. (d) Reduction in AAS adsorption in LS and HS. The unit conversion: 1 wt% = 10,000 ppm.

tion of anionic surfactants was not merely because of PA chelating divalent ions. This explanation was expected as the applied PA concentration compared to the containing divalent ions was much smaller, the chelating effect was not sufficient to explain the decreased binding of surfactants. However, the underlying mechanism for the reduction was still not clear on different mineral surfaces. As discussed above (Section 3.3), we proposed the charge screening mechanism for the reduction of AAS surfactant on calcite surfaces. It therefore makes sense to compare the adsorption capabilities of PA and AAS on mineral surfaces. Alumina is a Lewis acid and has strong interactions with Lewis bases, like PA and AAS. The PA charge screening effect (most PA adsorption) on alumina can be strongest, resulting in a lowest later AAS adsorption. But the situation on calcite and silica is different. In the presence of 50 mM $CaCl_2$, the maximal AAS adsorption on calcite is 23 Hz, while on silica is 30 Hz. It suggests that AAS has a higher affinity to silica than to calcite, indicating more adsorption sites on silica surfaces. AAS could still show a higher AAS adsorption on silica than on calcite after PA preflush (less reduction in AAS adsorption on silica). Therefore, it is more difficult to reduce AAS adsorption on silica compared to calcite. In this picture, PA reduced surfactant adsorption would follow the order of alumina > calcite > silica.

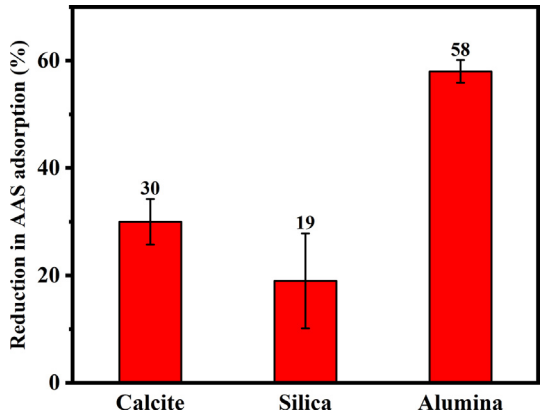

Fig. 7. Reduction in 0.15 wt% AAS adsorption on calcite, silica and alumina surfaces in HS condition and with the presence of 30 ppm PA, at pH 9.5 and room temperature. The unit conversion: 1 wt% = 10,000 ppm.

4. Conclusions

We have found that PA polyelectrolytes are able to act as sacrificial agent to reduce the adsorption of the anionic surfactant AAS to the mineral surfaces as deduced from QCM-D measurements, which were performed for the first time. This technique is relatively facile to screen different important experimental parameters (like ionic compositions and surface properties) and allows to perform real-time analysis of the surfactant adsorption behavior. It is also a good alternative to the traditional dynamic adsorption experiments done with time-consuming core flooding tests [30]. Our results demonstrated that the adsorption of AAS surfactant increased with increasing AAS concentration until a critical concentration, which can be described by the Langmuir isotherm. Adsorption of PA was a much slower process compared to AAS adsorption, and the process continued during our time of experimentation (90 min). Therefore, we have monitored the adsorption rates, instead of the amount adsorbed, as function of PA concentration. A higher PA concentration resulted in a higher adsorption rate. Calcium ions played a dominant role in the adsorption processes, where they acted as a bridging ion between the negatively charged surface and the negatively charged AAS or negatively charged PA. This interpretation was confirmed by DFT calculations. A higher calcium ion concentration resulted in a higher amount of adsorbed AAS and a higher rate of adsorption of PA. All adsorption phenomena of AAS and PA were found to be reversible. Increasing the NaCl concentration favored the AAS adsorption to calcite, likely due to a reduction of charges.

Since PA adsorption is much slower than AAS adsorption, it is of importance that, to be effective, the PA should be applied in a preflush, rather than applied in combination with the AAS. In doing so, the amount of AAS adsorbed can be reduced by 30% upon applying 30 ppm of PA. The PA from the preflush binds via also calcium ion bridging to the surface and lowers the overall number of binding sites for AAS adsorption. Changing the conditions from HS to LS, showed that the amount of AAS and PA adsorbed were lower, and that also that the reduction of AAS adsorption was lowered to 8%. In the absence of PA changing from HS to LS conditions already reduced the amount of AAS adsorbed by 50%. Addition of PA was relatively more beneficial for the HS conditions relative to the LS conditions. To further evaluate the potential of PA on different mineral surfaces, our results showed that PA reduced the adsorption of anionic surfactant on silica and alumina minerals

as well as calcite, yet it was not as effective in the case of silica as it was for calcite and alumina. It is expected that optimizing the surfactant injection conditions based on obtained results will minimize surfactant adsorption with reduced surfactant loss and thus contribute to develop more efficient flooding strategies in oil recovery.

CRediT authorship contribution statement

Zilong Liu: Conceptualization, Data curation, Formal analysis, Investigation, Methodology, Supervision, Validation, Writing - original draft. **Pegah Hedayati:** Conceptualization, Data curation, Formal analysis, Investigation, Methodology, Validation. **Murali K. Ghatkesar:** Investigation, Formal analysis. **Weichao Sun:** Data curation, Formal analysis, Investigation, Methodology. **Hayati Onay:** Formal analysis, Investigation. **Dirk Groenendijk:** Formal analysis, Funding acquisition, Project administration. **Johannes van Wunnik:** Formal analysis, Funding acquisition, Project administration, Writing - review & editing. **Ernst J.R. Sudhölter:** Conceptualization, Formal analysis, Funding acquisition, Project administration, Resources, Supervision, Writing - review & editing.

Declaration of Competing Interest

The authors declare that they have no known competing financial interests or personal relationships that could have appeared to influence the work reported in this paper.

Acknowledgments

The authors thank Dr. Mark Brewer (Shell Global Solutions) for providing surfactant samples, and for his active discussions and careful corrections. Technical assistance from Mr. Duco Bosma, Mr. Marcel Bus, and Mr. Ben Norder of TU Delft are highly appreciated. Financial support was provided by Shell Global Solutions and Science Foundation of China University of Petroleum, Beijing (no. 2462020BJRC007).

Appendix A. Supplementary data

Higher magnification SEM image of calcite surface; Viscosity results of different solutions; Adsorption of AAS surfactant with varying concentrations; Adsorption process of PA; Adsorption of AAS surfactant with varying $CaCl_2$ concentrations; Schematic presentation of co-injection and preflush methods; Different flooding methods for AAS surfactant adsorption in the presence and absence of PA. Supplementary data to this article can be found online at https://doi.org/10.1016/j.jcis.2020.11.090.

References

[1] G. Hirasaki, C.A. Miller, M. Puerto, Recent advances in surfactant EOR, SPE J. 16 (04) (2011) 889–907.
[2] M.S. Kamal, I.A. Hussein, A.S. Sultan, Review on surfactant flooding: phase behavior, retention, IFT, and field applications, Energy Fuels 31 (8) (2017) 7701–7720.
[3] L.W. Lake, R.T. Johns, W.R. Rossen, G.A. Pope, Fundamentals Enhanced Oil Recovery (2014).
[4] M. Tagavifar, S.H. Jang, H. Sharma, D. Wang, L.Y. Chang, K. Mohanty, G.A. Pope, Effect of PH on adsorption of anionic surfactants on limestone: experimental study and surface complexation modeling, Colloids Surf. Physicochem. Eng. Asp. 538 (2018) 549–558.
[5] S.D. Elias, A.M. Rabiu, O. Oluwaseun, B. Seima, Adsorption characteristics of surfactants on different petroleum reservoir materials, (2016).
[6] M.A. Ahmadi, S.R. Shadizadeh, Experimental investigation of a natural surfactant adsorption on shale-sandstone reservoir rocks: Static and dynamic conditions, Fuel 159 (C) (2015) 15–26.
[7] H. ShamsiJazeyi, R. Verduzco, G.J. Hirasaki, Reducing adsorption of anionic surfactant for enhanced oil recovery: Part Icompetitive adsorption mechanism, Colloids Surf. Physicochem. Eng. Asp. 453 (2014) 162–167.
[8] H. ShamsiJazeyi, R. Verduzco, G.J. Hirasaki, Reducing adsorption of anionic surfactant for enhanced oil recovery: Part II. Applied aspects, Colloids Surf. Physicochem. Eng. Asp. 453 (2014) 168–175.
[9] A. Durán-Álvarez, M. Maldonado-Domínguez, O. González-Antonio, C. Durán-Valencia, M. Romero-Ávila, F. Barragán-Aroche, S. López-Ramírez, Experimental-theoretical approach to the adsorption mechanisms for anionic, cationic, and zwitterionic surfactants at the calcite-water interface, Langmuir 32 (11) (2016) 2608–2616.
[10] S. Park, E.S. Lee, W.R.W. Sulaiman, Adsorption behaviors of surfactants for chemical flooding in enhanced oil recovery, J. Ind. Eng. Chem. 21 (2015) 1239–1245.
[11] D. Al Mahrouqi, J. Vinogradov, M.D. Jackson, Zeta potential of artificial and natural calcite in aqueous solution, Adv. Colloid Interface Sci. 240 (2017) 60–76.
[12] R. Zhang, P. Somasundaran, Advances in adsorption of surfactants and their mixtures at solid/solution interfaces, Adv. Colloid Interface Sci. 123 (2006) 213–229.
[13] H. Mahani, R. Menezes, S. Berg, A. Fadili, R. Nasralla, D. Voskov, V. Joekar-Niasar, Insights into the impact of temperature on the wettability alteration by low salinity in carbonate rocks, Energy Fuels 31 (8) (2017) 7839–7853.
[14] S. Solairaj, C. Britton, D.H. Kim, U. Weerasooriya, G.A. Pope, Measurement and analysis of surfactant retention, in: SPE Improved Oil Recovery Symposium, Society of Petroleum Engineers, 2012.
[15] P. Somasundaran, L. Zhang, Adsorption of surfactants on minerals for wettability control in improved oil recovery processes, J. Pet. Sci. Eng. 52 (1–4) (2006) 198–212.
[16] K. Hu, A.J. Bard, Characterization of adsorption of sodium dodecyl sulfate on charge-regulated substrates by atomic force microscopy force measurements, Langmuir 13 (20) (1997) 5418–5425.
[17] J.J. Hamon, A. Striolo, R.F. Tabor, B.P. Grady, AFM force mapping analysis of an adsorbed surfactant above and below the CMC, Langmuir 34 (25) (2018) 7223–7239.
[18] M. Akbar, B. Vissapragada, A.H. Alghamdi, D. Allen, M. Herron, A. Carnegie, D. Dutta, J.-R. Olesen, R.D. Chourasiya, D. Logan, A snapshot of carbonate reservoir evaluation, Oilfield Rev. 12 (4) (2000) 20–21.
[19] A. Al-Khafaji, A. Neville, M. Wilson, D. Wen, Effect of low salinity on the oil desorption efficiency from calcite and silica surfaces, Energy Fuels 31 (11) (2017) 11892–11901.
[20] G. Hirasaki, D.L. Zhang, Surface chemistry of oil recovery from fractured, oil-wetcarbonate formations, Spe J. 9 (02) (2004) 151–162.
[21] T. Austad, A. RezaeiDoust, T. Puntervold, Chemical mechanism of low salinity water flooding in sandstone reservoirs, in: SPE improved oil recovery symposium, Society of Petroleum Engineers, 2010, p. 129767.
[22] M. Lashkarbolooki, S. Ayatollahi, M. Riazi, Mechanistical study of effect of ions in smart water injection into carbonate oil reservoir, Process Saf. Environ. Prot. 105 (2017) 361–372.
[23] R.M. Haaring, N. Kumar, D. Bosma, L. Poltorak, E.J. Sudholter, Electrochemically-assisted deposition of calcite for application in surfactant adsorption studies, Energy Fuels 33 (2) (2019) 805–813.
[24] Z.L. Liu, T. Rios-Carvajal, M.P. Andersson, M. Ceccato, S.L.S. Stipp, T. Hassenkam, Insights into the pore-scale mechanism for the low-salinity effect: implications for enhanced oil recovery, Energy Fuels 32 (12) (2018) 12081–12090.
[25] Z. Liu, T. Rios-Carvajal, M.P. Andersson, S. Stipp, T. Hassenkam, Ion effects on molecular interaction between graphene oxide and organic molecules, Environ. Sci. Nano 6 (7) (2019) 2281–2291.
[26] E.J. Wanless, W.A. Ducker, Weak influence of divalent ions on anionic surfactant surface-aggregation, Langmuir 13 (6) (1997) 1463–1474.
[27] M. Budhathoki, S.H.R. Barnee, B.-J. Shiau, J.H. Harwell, Improved oil recovery by reducing surfactant adsorption with polyelectrolyte in high saline brine, Colloids Surf. Physicochem. Eng. Asp. 498 (2016) 66–73.
[28] A.M. Johannessen, K. Spildo, Enhanced oil recovery (EOR) by combining surfactant with low salinity injection, Energy Fuels 27 (10) (2013) 5738–5749.
[29] M. Nourani, T. Tichelkamp, B. Gaweł, G. Øye, Desorption of crude oil components from silica and aluminosilicate surfaces upon exposure to aqueous low salinity and surfactant solutions, Fuel 180 (2016) 1–8.
[30] A. Lager, K.J. Webb, C.J.J. Black, Impact of brine chemistry on oil recovery, in: IOR 2007-14th European Symposium on Improved Oil Recovery, (2007).
[31] W.L. Ng, D. Rana, G.H. Neale, V. Hornof, Physicochemical behavior of mixed surfactant systems: petroleum sulfonate and lignosulfonate, J. Appl. Polym. Sci. 88 (4) (2003) 860–865.
[32] H. Shamsijazeyi, G. Hirasaki, R. Verduzco, Sacrificial Agent for Reducing Adsorption of Anionic Surfactants, in: SPE International Symposium on Oilfield Chemistry, Society of Petroleum Engineers, (2013), p. 164061.
[33] K. Esumi, M. Iitaka, Y. Koide, Simultaneous adsorption of poly (ethylene oxide) and cationic surfactant at the silica/water interface, J. Colloid Interface Sci. 208 (1) (1998) 178–182.
[34] J.S. Weston, J.H. Harwell, B.J. Shiau, M. Kabir, Disrupting admicelle formation and preventing surfactant adsorption on metal oxide surfaces using sacrificial polyelectrolytes, Langmuir 30 (22) (2014) 6384–6388.

[35] K. He, Z. Yue, C. Fan, L. Xu, Minimizing surfactant adsorption using polyelectrolyte based sacrificial agent: a way to optimize surfactant performance in unconventional formations, in: SPE international symposium on oilfield chemistry, Society of Petroleum Engineers, 2015, p. 173750.
[36] S.B. Velegol, R.D. Tilton, Specific counterion effects on the competitive co-adsorption of polyelectrolytes and ionic surfactants, J. Colloid Interface Sci. 249 (2) (2002) 282–289.
[37] L. Daoshan, L. Shouliang, L. Yi, W. Demin, The effect of biosurfactant on the interfacial tension and adsorption loss of surfactant in ASP flooding, Colloids Surf. Physicochem. Eng. Asp. 244 (1–3) (2004) 53–60.
[38] X. Li, Y. Bai, H. Sui, L. He, Understanding desorption of oil fractions from mineral surfaces, Fuel 232 (2018) 257–266.
[39] S. Kelesoglu, S. Volden, M. Kes, J. Sjoblom, Adsorption of naphthenic acids onto mineral surfaces studied by quartz crystal microbalance with dissipation monitoring (QCM-D), Energy Fuels 26 (8) (2012) 5060–5068.
[40] S. Adkins, P.J. Liyanage, P. Arachchilage, W.P. Gayani, T. Mudiyanselage, U. Weerasooriya, G.A. Pope, A new process for manufacturing and stabilizing high-performance EOR surfactants at low cost for high-temperature, high-salinity oil reservoirs, in: SPE Improved Oil Recovery Symposium, Society of Petroleum Engineers, 2010, p. 129923.
[41] H.H. Teng, P.M. Dove, C.A. Orme, J.J. De Yoreo, Thermodynamics of calcite growth: baseline for understanding biomineral formation, Science 282 (5389) (1998) 724–727.
[42] G. Sauerbrey, Verwendung von Schwingquarzen Zur Wägung Dünner Schichten Und Zur Mikrowägung, Z. Für Phys. 155 (2) (1959) 206–222.
[43] K.K. Kanazawa, J.G. Gordon, Frequency of a quartz microbalance in contact with liquid, Anal. Chem. 57 (8) (1985) 1770–1771.
[44] M. Rodahl, B. Kasemo, On the measurement of thin liquid overlayers with the quartz-crystal microbalance, Sens. Actuators Phys. 54 (1–3) (1996) 448–456.
[45] N.-J. Cho, J.N. D'Amour, J. Stalgren, W. Knoll, K. Kanazawa, C.W. Frank, Quartz resonator signatures under newtonian liquid loading for initial instrument check, J. Colloid Interface Sci. 315 (1) (2007) 248–254.
[46] R. Ahlrichs, M. Bär, M. Häser, H. Horn, C. Kölmel, Electronic structure calculations on workstation computers: the program system turbomole, Chem. Phys. Lett. 162 (3) (1989) 165–169.
[47] J.P. Perdew, Density-functional approximation for the correlation energy of the inhomogeneous electron gas, Phys. Rev. B 33 (12) (1986) 8822.
[48] A.D. Becke, Density-functional exchange-energy approximation with correct asymptotic behavior, Phys. Rev. A 38 (6) (1988) 3098.
[49] A. Schäfer, H. Horn, R. Ahlrichs, Fully optimized contracted gaussian basis sets for atoms Li to Kr, J. Chem. Phys. 97 (4) (1992) 2571–2577.
[50] A. Klamt, G. Schüürmann, COSMO: A new approach to dielectric screening in solvents with explicit expressions for the screening energy and its gradient, J. Chem. Soc. Perkin Trans. 2 (5) (1993) 799–805.
[51] B. Lorenz, M. Ceccato, M.P. Andersson, S. Dobberschütz, J.D. Rodriguez-Blanco, K.N. Dalby, T. Hassenkam, S.L.S. Stipp, Salinity-Dependent adhesion response properties of aluminosilicate (k-Feldspar) surfaces, Energy Fuels 31 (5) (2017) 4670–4680.
[52] J. Collins, D. Funfschilling, M. Dennin, Langmuir Blodgett films of arachidic acid and a nematic liquid crystal: characterization and use in homeotropic alignment, Thin Solid Films 496 (2) (2006) 601–605.
[53] Z. Liu, M.K. Ghatkesar, E.J. Sudholter, B. Singh, N. Kumar, Understanding the cation dependent surfactant adsorption on clay minerals in oil recovery, Energy Fuels 33 (12) (2019) 12319–12329.
[54] P. Kele, J. Orbulescu, S.V. Mello, M. Mabrouki, R.M. Leblanc, Langmuir and Langmuir– Blodgett Film characterization of a new amphiphilic coumarin derivative, Langmuir 17 (23) (2001) 7286–7290.
[55] R.E. Bulo, D. Donadio, A. Laio, F. Molnar, J. Rieger, M. Parrinello, "Site Binding" of Ca^{2+} Ions to polyacrylates in water: a molecular dynamics study of coiling and aggregation, Macromolecules 40 (9) (2007) 3437–3442.
[56] F. Fantinel, J. Rieger, F. Molnar, P. Hübler, Complexation of polyacrylates by Ca2 + ions. Time-resolved studies using attenuated total reflectance fourier transform infrared dialysis spectroscopy, Langmuir 20 (7) (2004) 2539–2542.
[57] T. Swift, C.C. Seaton, S. Rimmer, Poly (acrylic acid) interpolymer complexes, Soft Matter 13 (46) (2017) 8736–8744.
[58] R. Schweins, K. Huber, Collapse of sodium polyacrylate chains in calcium salt solutions, Eur. Phys. J. E 5 (1) (2001) 117–126.
[59] D.J. Sparks, M.E. Romero-González, E. El-Taboni, C.L. Freeman, S.A. Hall, G. Kakonyi, L. Swanson, S.A. Banwart, J.H. Harding, Adsorption of poly acrylic acid onto the surface of calcite: an experimental and simulation study, Phys. Chem. Chem. Phys. 17 (41) (2015) 27357–27365.
[60] Z. Liu, P. Hedayati, E.J. Sudhölter, R. Haaring, A.R. Shaik, N. Kumar, Adsorption behavior of anionic surfactants to silica surfaces in the presence of calcium ion and polystyrene sulfonate, Colloids Surf. Physicochem. Eng. Asp. 602 (2020) 125074.
[61] G.-Q. Tang, N.R. Morrow, Influence of brine composition and fines migration on crude oil/brine/rock interactions and oil recovery, J. Pet. Sci. Eng. 24 (2–4) (1999) 99–111.